SCIENCE CHINA
Information Sciences

• Supplementary File •

Finite-time H_∞ control and energy cost optimization for nonlinear delayed systems through switching analysis and interval matrix method

Guici Chen[1*], Huimin Zeng[1], Song Zhu[2], Shiping Wen[3] & Junhao Hu[4]

[1]*Hubei Province Key Laboratory of System Science in Metallurgical Process, Wuhan University of Science and Technology, Wuhan 430065, China;*
[2]*School of Mathematics, China University of Mining and Technology, Xuzhou, 221116, China;*
[3]*Centre for Artifcial Intelligence, University of Technology Sydney, Sydney, 2007, Australia;*
[4]*School of Mathematics and Statistics, South-Central Minzu University, Wuhan 430074, China*

Appendix A Interval matrix method analysis and preparations

Notations. Cross this paper, $\dot{a}(t)$ stands for the derivative of $a(t)$ with respect to t, and $\mathbb{R}^n$ indicates n dimensional Euclidean space. O^T and O^{-1} denote the transpose of O and the inverse of O, respectively. $*$ implies a transposed term. $\lambda_{\max}(M)$ and $\lambda_{\min}(M)$ represent the maximum and minimum eigenvalues of the matrix M, respectively. $co[m,n]$ means the convex combination of m and n.

IMM analysis. Below we take an example of the coefficient matrix $\mathcal{A}(t)$ with parameters varying over time. $\mathcal{A}(t)$ can be analyzed as $(a_{kw}(t))_{n\times n} \in co[\hat{\mathcal{A}}, \check{\mathcal{A}}]$, with $k,w = \{1,2,\ldots,n\}$. Here, $\check{a}_{kw} = max\{a_{kw}(t)\}$, $\hat{a}_{kw} = min\{a_{kw}(t)\}$, $\forall t \in [t_0, T_f]$, $\hat{a}_{kw} \leqslant a_{kw}(t) \leqslant \check{a}_{kw}$. Define $\hat{\mathcal{A}} = (\hat{a}_{kw})_{n\times n}$, $\check{\mathcal{A}} = (\check{a}_{kw})_{n\times n}$. Due to convexity, it is natural to derive

$$a_{kw}(t) = \frac{1}{2}(\check{a}_{kw} + \hat{a}_{kw}) + \frac{\lambda_{kw}(t)}{2}(\check{a}_{kw} - \hat{a}_{kw}) = a_{kw} + \lambda_{kw}(t)\bar{a}_{kw},$$

where $a_{kw} = \frac{1}{2}(\check{a}_{kw} + \hat{a}_{kw})$, $\bar{a}_{kw} = \frac{1}{2}(\check{a}_{kw} - \hat{a}_{kw})$. Also, it indicates $\mathcal{A} = (a_{kw})_{n\times n}$, $\Delta\mathcal{A}(t) = (\lambda_{kw}(t)\bar{a}_{kw})_{n\times n}$, $\lambda_{kw}(t) \in [-1,1]$. $\Delta\mathcal{A}(t)$ is shown as a split of the matrices $\Delta\mathcal{A}(t) = H_a L_a(t) M_a$, $L_a^T(t)L_a(t) \leqslant I_{n^2\times n^2}$. Obviously, one easily follows that

$$\mathcal{A}(t) \in co[\hat{\mathcal{A}}, \check{\mathcal{A}}] = \mathcal{A} + H_a L_a(t) M_a,$$

with

$$L_a(t) = diag\{\lambda_{11}(t), ..., \lambda_{1n}(t), ..., \lambda_{n1}(t), ..., \lambda_{nn}(t)\}_{n^2\times n^2}, H_a = [\sqrt{\bar{a}_{11}}\chi_1, ..., \sqrt{\bar{a}_{1n}}\chi_1, ..., \sqrt{\bar{a}_{n1}}\chi_n, ..., \sqrt{\bar{a}_{nn}}\chi_n]_{n\times n^2},$$
$$M_a = [\sqrt{\bar{a}_{11}}\chi_1^T, ..., \sqrt{\bar{a}_{1n}}\chi_n^T, ..., \sqrt{\bar{a}_{n1}}\chi_1^T, ..., \sqrt{\bar{a}_{nn}}\chi_n^T]_{n^2\times n},$$

where $\chi_r^T = (0, ..., \underbrace{1}_{rth}, ..., 0)$, which denotes a row vector wherein the rth element is 1 and all remaining elements assume 0. Therefore, we can re-express NDSs

$$\begin{cases} \mathrm{d}\mathsf{x}(t) \in \{co[\hat{\mathcal{A}}, \check{\mathcal{A}}]\mathsf{x}(t) + co[\hat{\mathcal{A}}_d, \check{\mathcal{A}}_d]\mathsf{x}(t-\iota(t)) + f(\mathsf{x}(t),t) + g(\mathsf{x}(t-\iota(t)),t) + \mathcal{B}v(t) + \mathcal{G}u(t)\}\mathrm{d}t, \\ \mathsf{z}(t) \in co[\hat{E}, \check{E}]\mathsf{x}(t) + \mathcal{W}v(t). \end{cases} \tag{A1}$$

When focusing on the ith subsystem, one can express the subsystem coefficients below

$$\mathcal{A}_i(t) \in co[\hat{\mathcal{A}}_i, \check{\mathcal{A}}_i] = \mathcal{A}_i + H_{ai}L_{ai}(t)M_{ai}; \mathcal{A}_{di}(t) \in co[\hat{\mathcal{A}}_{di}, \check{\mathcal{A}}_{di}] = \mathcal{A}_{di} + H_{di}L_{di}(t)M_{di};$$
$$E_i(t) \in co[\hat{E}_i, \check{E}_i] = E_i + H_{ei}L_{ei}(t)M_{ei}.$$

Substituting the above equations into NDSSs yields

$$\begin{cases} \mathrm{d}\mathsf{x}(t) \in \{[\mathcal{A}_i + H_{ai}L_{ai}(t)M_{ai} + \mathcal{G}K_i]\mathsf{x}(t) + [\mathcal{A}_{di} + H_{di}L_{di}(t)M_{di}]\mathsf{x}(t-\iota(t)) + f_i(\mathsf{x}(t),t) + g_i(\mathsf{x}(t-\iota(t)),t) + \mathcal{B}v(t)\}\mathrm{d}t, \\ \mathsf{z}(t) \in [E_i + H_{ei}L_{ei}(t)M_{ei}]\mathsf{x}(t) + \mathcal{W}v(t). \end{cases} \tag{A2}$$

* Corresponding author (email: chenguici@wust.edu.cn)

Remark 1. Time-varying characteristics are typically viewed as detrimental in analyzing and designing control systems. [1] exploited the DLMIs technique and state transition matrix to seek the optimal solution over the set of all permissible matrix-valued functions, which caused a significant computational burden. [2] straightforwardly converting time-varying systems into uncertain systems with time-varying parameters may introduce conservatism when confronted with sudden fluctuations in time-varying parameters. With the proposed IMM in conjunction with switching analysis, one can further transform time-varying systems into uncertain subsystems with time-varying parameters which can implement more accurate analysis and control by considering the time-varying parameter control intervals of subsystems consisting of both their minimum and maximum values, and representing the interval parameters as convex combinations, i.e., time-varying parameters of the subsystems are contained in a closure.

Assumption 1. The time-varying exogenous disturbance $v(t) \in \mathbb{R}^v$ satisfies the following condition for scalar $\beta \geqslant 0$

$$\int_0^{T_f} v^T(s)v(s)\mathrm{d}s \leqslant \beta.$$

Assumption 2. For known nonlinear functions $f(\cdot,\cdot)$, $g(\cdot,\cdot)$, which are presumed to satisfy the global Lipschitz condition, when focusing on $\sigma(t) = i$, there exist constants l_{1i}, $l_{2i} \geqslant 0$ such that inequalities below hold

$$|f_i(\varrho_1, t) - f_i(\varrho_2, t)|^2 \leqslant l_{1i}|\varrho_1 - \varrho_2|^2; \quad |g_i(\vartheta_1, t) - g_i(\vartheta_2, t)|^2 \leqslant l_{2i}|\vartheta_1 - \vartheta_2|^2,$$

where $f_i(0,t) = 0, g_i(0,t) = 0$ are assumed to be satisfied.

Lemma 1. ([3]). If $\acute{\Upsilon}_{11}$, $\acute{\Upsilon}_{22}$ are invertible matrices for a symmetric matrix $\acute{\Upsilon} = \begin{bmatrix} \acute{\Upsilon}_{11} & \acute{\Upsilon}_{12} \\ * & \acute{\Upsilon}_{22} \end{bmatrix}$, the following inequalities stand as equivalent propositions

$$(1)\acute{\Upsilon} < 0; \quad (2)\acute{\Upsilon}_{11} < 0, \acute{\Upsilon}_{22} - \acute{\Upsilon}_{12}^T\acute{\Upsilon}_{11}^{-1}\acute{\Upsilon}_{12} < 0; \quad (3)\acute{\Upsilon}_{22} < 0, \acute{\Upsilon}_{11} - \acute{\Upsilon}_{12}\acute{\Upsilon}_{22}^{-1}\acute{\Upsilon}_{12}^T < 0.$$

Lemma 2. ([4]). For a given matrix $U \in R^{n\times n}$ which is symmetric, and real matrices M, H with appropriate dimensions, for the following inequality

$$U + HL(t)M + M^T L^T(t)H^T < 0,$$

if there exists $L^T(t)L(t) < I$, then one has a scalar $\epsilon > 0$ satisfying

$$U + \epsilon M^T M + \epsilon^{-1} HH^T < 0.$$

Definition 1. (Finite-time boundedness, FTB [5]). Given positive scalars T_f, d_1, β, where $d_1 < d_2$, a switching signal $\sigma(t)$, a matrix $\mathsf{R} > 0$ and $v(t)$ following Assumption 1, the systems are considered to be FTB regarding (d_1, d_2, β, T_f, R, σ) when $u(t) \equiv 0$, satisfying

$$\sup_{s\in[-\iota,0]} \{\mathsf{x}^T(s)\mathsf{R}\mathsf{x}(s)\} \leqslant d_1 \Longrightarrow \mathsf{x}^T(t)\mathsf{R}\mathsf{x}(t) < d_2, \forall t \in [0, T_f]. \tag{A3}$$

Definition 2. (Finite-time H_∞ boundedness, H_∞ FTB [6]) Given positive scalars T_f, d_1, β, a switching signal $\sigma(t)$, and a matrix $\mathsf{R} > 0$, the systems are deemed to be H_∞ FTB regarding (d_1, d_2, β, T_f, R, σ) with $u(t) \equiv 0$, if the following conditions hold

(i) The systems are FTB.

(ii) $\mathsf{z}(t)$ under zero initial condition satisfies below

$$\int_0^{T_f} \mathsf{z}^T(s)\mathsf{z}(s)\mathrm{d}s < \gamma^2 \int_0^{T_f} v^T(s)v(s)\mathrm{d}s, \tag{A4}$$

with the disturbance input $v(t)$ meets Assumption 1, and γ is a positive constant.

Definition 3. (Finite-time H_∞ Control, H_∞ FTC [6]). The systems are referred as finite-time H_∞ controllable with H_∞ performance index, if there exists a control input $u(t)$ on $[0, T_f]$, and the closed-loop systems being H_∞ FTB.

Appendix B Proof of Theorem 1

Theorem 1. For given several positive constants d_1, β, T_f, m, α, l_{1i}, l_{2i} and a matrix $\mathsf{R} > 0$, the NDSSs achieve FTB regarding (d_1, d_2, β, T_f, R, σ), if there exist positive scalars $\mu_i > 1$, d_2, ϵ_{fi}, ϵ_{gi}, and positive definite matrices P_i, S_i, satisfying

$$\begin{bmatrix} \Gamma & \Xi \\ * & \Theta \end{bmatrix} < 0, \tag{B1}$$

$$\Omega < 0, \tag{B2}$$

$$P_i < \mu_i P_j, S_i < \mu_i S_j, j = i-1, \forall i, j \in \mathbb{M}, \tag{B3}$$

where

$$\Gamma_{1,1} = P_i\mathcal{A}_i(t) + \mathcal{A}_i^T(t)P_i + S_i + \epsilon_f P_i^2 + \epsilon_g P_i^2 - \alpha P_i, \Gamma_{1,2} = P_i\mathcal{A}_{di}(t), \Gamma_{1,3} = P_i\mathcal{B}, \Gamma_{2,2} = -(1-h)\mathrm{e}^{\alpha\iota}S_i, \Gamma_{3,3} = -\alpha I,$$
$$\Xi = \begin{pmatrix} \sqrt{l_{1i}}I & 0 & 0 \\ 0 & \sqrt{l_{2i}}I & 0 \end{pmatrix}^T, \Theta = diag\{-\epsilon_{fi}I, -\epsilon_{gi}I\}, \Omega_{1,1} = (\lambda_1 + \iota\mathrm{e}^{\alpha\iota}\lambda_2)d_1 + \alpha\beta, \Omega_{1,2} = \sqrt{\lambda_3 d_2}, \Omega_{2,2} = \mathrm{e}^{\alpha T_f}\prod_{i=2}^{m}\mu_i.$$

Proof. The following multiple Lyapunov functions (MLFs) candidates are chosen for NDSSs

$$V_i(\mathsf{x}_t, t) = \sum_{\kappa=1}^{2} V_{\kappa i}(\mathsf{x}_t, t), \tag{B4}$$

with each $V_{\kappa i}(t)$ is given below

$$V_{1i}(\mathsf{x}_t, t) = \mathsf{x}^T(t)P_i\mathsf{x}(t), \quad V_{2i}(\mathsf{x}_t, t) = \int_{t-\iota(t)}^{t} \mathrm{e}^{\alpha(t-\theta)}\mathsf{x}^T(\theta)S_i\mathsf{x}(\theta)\mathrm{d}\theta.$$

Then, the derivative of $V_{\kappa i}(t)$ along the NDSSs, it obtains

$$\dot{V}_{1i}(\mathsf{x}_t, t) = 2\mathsf{x}^T(t)P_i[\mathcal{A}_i(t)\mathsf{x}(t) + \mathcal{A}_{di}(t)\mathsf{x}(t-\iota(t)) + f_i(\mathsf{x}(t), t) + g_i(\mathsf{x}(t-\iota(t)), t) + \mathcal{B}v(t)],$$
$$\dot{V}_{2i}(\mathsf{x}_t, t) = \mathsf{x}^T(t)S_i\mathsf{x}(t) - \mathrm{e}^{\alpha\iota(t)}(1-\dot{\iota}(t))\mathsf{x}^T(t-\iota(t))S_i\mathsf{x}(t-\iota(t)) + \alpha\int_{t-\iota(t)}^{t}\mathrm{e}^{\alpha(t-\theta)}\mathsf{x}^T(\theta)S_i\mathsf{x}(\theta)\mathrm{d}\theta.$$

The combination of Assumption 2 and Lemma 2, one easily acquires

$$\begin{aligned}\sum_{\kappa=1}^{2}\dot{V}_{\kappa i}(\mathsf{x}_t, t) \leqslant & \mathsf{x}^T(t)(P_i\mathcal{A}_i(t) + \mathcal{A}_i^T(t)P_i + S_i + \epsilon_{fi}P_i^2 + \epsilon_{gi}P_i^2 + \epsilon_{fi}^{-1}l_{1i}I)\mathsf{x}(t) + \mathsf{x}^T(t)P_i\mathcal{A}_{di}(t)\mathsf{x}(t-\iota(t)) \\ & + \mathsf{x}^T(t-\iota(t))\mathcal{A}_{di}^T(t)P_i\mathsf{x}(t) + \mathsf{x}^T(t-\iota(t))(\epsilon_{gi}^{-1}l_{2i}I - (1-h)\mathrm{e}^{\alpha\iota}S_i)\mathsf{x}(t-\iota(t)) + \mathsf{x}^T(t)P_i\mathcal{B}v(t) \\ & + v^T(t)\mathcal{B}^TP_i\mathsf{x}(t) + \alpha\int_{t-\iota(t)}^{t}\mathrm{e}^{\alpha(t-\theta)}\mathsf{x}^T(\theta)S_i\mathsf{x}(\theta)\mathrm{d}\theta.\end{aligned} \tag{B5}$$

Thus, from inequalities (B4)-(B5), it's obviously reached

$$\dot{V}_i(\mathsf{x}_t, t) - \alpha V_i(\mathsf{x}_t, t) - \alpha v^T(t)v(t) \leqslant \breve{\chi}^T(t)\Lambda\breve{\chi}(t),$$

where $\breve{\chi}^T(t) = [\mathsf{x}^T(t), \mathsf{x}^T(t-\iota(t)), v^T(t)]$, $\Lambda = \begin{bmatrix} \varphi_{11} & P_i\mathcal{A}_{di}(t) & P_i\mathcal{B} \\ * & \varphi_{22} & 0 \\ * & * & -\alpha I \end{bmatrix}$,

with $\varphi_{11} = P_i\mathcal{A}_i(t) + \mathcal{A}_i^T(t)P_i + S_i + \epsilon_{fi}P_i^2 + \epsilon_{gi}P_i^2 + \epsilon_{fi}^{-1}l_{1i}I - \alpha P_i$, $\varphi_{22} = \epsilon_{gi}^{-1}l_{2i}I - (1-h)\mathrm{e}^{\alpha\iota}S_i$.

By considering Lemma 1, the condition (B1) implies that $\Lambda < 0$. Hence, we have

$$\dot{V}_i(\mathsf{x}_t, t) < \alpha V_i(\mathsf{x}_t, t) + \alpha v^T(t)v(t). \tag{B6}$$

Integrating inequality (B6) for $t \in [t_p, t_{p+1})$

$$V_{\sigma(t)}(\mathsf{x}_t, t) < \mathrm{e}^{\alpha(t-t_p)}V_{\sigma(t_p)}(\mathsf{x}_t, t) + \int_{t_p}^{t}\alpha\mathrm{e}^{\alpha(t-s)}v^T(s)v(s)\mathrm{d}s. \tag{B7}$$

It follows from the condition (B3) that

$$V_i(\mathsf{x}_{t_p}, t_p) < \mu_i V_j(\mathsf{x}_{t_p^-}, t_p^-). \tag{B8}$$

According to [7] and [8], one obtains that

$$\begin{aligned}V_i(\mathsf{x}_t, t) &< \prod_{i=2}^{m}\mu_i\mathrm{e}^{\alpha(t-0)}V_{\sigma(0)}(\mathsf{x}_0, 0) + \alpha\prod_{i=2}^{m}\mu_i\int_0^t\mathrm{e}^{\alpha(t-s)}v^T(s)v(s)\mathrm{d}s \\ &< \prod_{i=2}^{m}\mu_i\mathrm{e}^{\alpha T_f}[V_{\sigma(0)}(\mathsf{x}_0, 0) + \alpha\int_0^{T_f}v^T(s)v(s)\mathrm{d}s] < \prod_{i=2}^{m}\mu_i\mathrm{e}^{\alpha T_f}[V_{\sigma(0)}(\mathsf{x}_0, 0) + \alpha\beta].\end{aligned} \tag{B9}$$

Then, let $\bar{P}_i = \mathsf{R}^{-\frac{1}{2}}P_i\mathsf{R}^{-\frac{1}{2}}$, $\bar{S}_i = \mathsf{R}^{-\frac{1}{2}}S_i\mathsf{R}^{-\frac{1}{2}}$

$$V_{\sigma(0)}(\mathsf{x}_0, 0) = \mathsf{x}^T(0)P_{\sigma(0)}\mathsf{x}(0) + \int_{-\iota(0)}^{0}\mathrm{e}^{-\alpha\theta}\mathsf{x}^T(\theta)S_{\sigma(0)}\mathsf{x}(\theta)\mathrm{d}\theta \leqslant (\lambda_1 + \iota\mathrm{e}^{\alpha\iota}\lambda_2)d_1. \tag{B10}$$

From the other side, we have

$$V_i(\mathsf{x}_t,t) > \mathsf{x}^T(t)P_i\mathsf{x}(t) \geqslant \lambda_3\mathsf{x}^T(t)\mathsf{R}\mathsf{x}(t), \tag{B11}$$

where $\lambda_1 = max\{\lambda_{max}(\bar{P}_i)\}$, $\lambda_2 = max\{\lambda_{max}(\bar{S}_i)\}$, $\lambda_3 = min\{\lambda_{min}(\bar{P}_i)\}$, $\forall i \in \mathbb{M}$.

By inequalities (B9)-(B11), it's easily got

$$\mathsf{x}^T(t)\mathsf{R}\mathsf{x}(t) < \frac{V_i(\mathsf{x}_t,t)}{\lambda_3} < \frac{\mathrm{e}^{\alpha T_f}\prod_{i=2}^{m}\mu_i[(\lambda_1+\iota\mathrm{e}^{\alpha\iota}\lambda_2)d_1+\alpha\beta]}{\lambda_3}. \tag{B12}$$

Therefore, from (B2), we have the following inequality

$$\mathsf{x}^T(t)\mathsf{R}\mathsf{x}(t) < d_2. \tag{B13}$$

From the above analysis and Definition 1, we conclude that NDSSs is FTB to (d_1, d_2, β, T_f, R, σ). This ends the proof.

Remark 2. It provides a series of matrix sufficient conditions for NDSSs in Theorem 1 to retain FTB from the perspective of switching analysis. The construction of MLFs with time delays and the application of some inequality techniques yield the sufficient condition (B1) for a more comprehensive discussion of subsystems, and the matrix condition (B3) to further constrains MLFs. On the other hand, as switching subsystems considered in this paper are converted from time-varying systems by performing switching analysis, therefore the switching number of each subsystem remains unique over $[0, T_f]$. Consequently, the common switching strategies ADT [7], and MDADT [8] are not suitable for this work. Instead, we introduce two switching strategies to compute the switching points in Appendix E.

Appendix C Proof of Theorem 2

A comprehensive exploration of the conditions is given to guarantee that the NDSSs achieve H_∞ FTB, and H_∞ performance index is also derived following the results of Theorem 2.

Theorem 2. For given some positive constants d_1, β, T_f, m, α, l_{1i}, l_{2i}, γ, the NDSSs achieve H_∞ FTB with respect to (d_1, d_2, β, T_f, R, σ) by setting H_∞ performance index $\gamma^\star = (\mathrm{e}^{\alpha T_f}\prod_{i=2}^{m}\mu_i)^{\frac{1}{2}}\gamma$, if there exist positive scalars $\mu_i > 1$, d_2, ϵ_{fi}, ϵ_{gi}, and positive definite matrices P_i, S_i, such that

$$\begin{bmatrix}\Pi & \acute{\Xi}\\ * & \Theta\end{bmatrix} < 0, \tag{C1}$$

$$\tilde{\Omega} < 0, \tag{C2}$$

$$P_i < \mu_i P_j, S_i < \mu_i S_j, j = i-1, \forall i,j \in \mathbb{M}, \tag{C3}$$

where

$$\Pi_{1,1} = P_i\mathcal{A}_i(t) + \mathcal{A}_i^T(t)P_i + S_i + \epsilon_{fi}P^2 + \epsilon_{gi}P^2 - \alpha P_i, \Pi_{1,2} = P_i\mathcal{A}_{di}(t), \Pi_{1,3} = P_i\mathcal{B}, \Pi_{1,4} = E_i^T(t),$$

$$\Pi_{2,2} = -(1-h)\mathrm{e}^{\alpha\iota}S_i, \Pi_{3,3} = -\gamma^2 I, \Pi_{3,4} = \mathcal{W}^T, \Pi_{4,4} = -I, \acute{\Xi} = \begin{pmatrix}\sqrt{l_{1i}}I & 0 & 0 & 0\\ 0 & \sqrt{l_{2i}}I & 0 & 0\end{pmatrix}^T,$$

$$\Theta = diag\{-\epsilon_{fi}I, -\epsilon_{gi}I\}, \tilde{\Omega}_{1,1} = (\lambda_1+\iota\mathrm{e}^{\alpha\iota}\lambda_2)d_1 + \gamma^2\beta, \tilde{\Omega}_{1,2} = \sqrt{\lambda_3 d_2}, \tilde{\Omega}_{2,2} = \mathrm{e}^{\alpha T_f}\prod_{i=2}^{m}\mu_i.$$

Proof. Building on the matrix conditions of Theorem 1 for further investigation, we will prove that the H_∞ FTB and solve H_∞ performance index of NDSSs with the zero initial condition.

Denote $\mathcal{S}(v_t,\mathsf{z}_t) = \gamma^2 v^T(t)v(t) - \mathsf{z}^T(t)\mathsf{z}(t)$. Similarly as the method of Theorem 1, one yields

$$\dot{V}_i(\mathsf{x}_t,t) - \alpha V_i(\mathsf{x}_t,t) - \mathcal{S}(v_t,\mathsf{z}_t) \leqslant \breve{\chi}^T(t)\Phi\breve{\chi}(t),$$

where $\breve{\chi}^T(t) = [\mathsf{x}^T(t), \mathsf{x}^T(t-\iota(t)), v^T(t)]$, and employing Lemma 1, it's got

$$\Phi = \begin{bmatrix}\varphi_{11} & P_i\mathcal{A}_{di}(t) & P_i\mathcal{B} & E_i^T(t)\\ * & \varphi_{22} & 0 & 0\\ * & * & -\gamma^2 I & \mathcal{W}^T\\ * & * & * & -I\end{bmatrix},$$

with φ_{11} and φ_{22} have been described in Theorem 1.

Along with the proof of Theorem 1, we obtain

$$V_i(t) < \mathrm{e}^{\alpha t}\prod_{i=2}^{m}\mu_i V_{\sigma(0)}(\mathsf{x}_0,0)+\prod_{i=2}^{m}\mu_i\int_0^t \mathrm{e}^{\alpha(t-s)}\mathcal{S}(s)\mathrm{d}s. \tag{C4}$$

Following $V_{\sigma(0)}(\mathsf{x}_0,0)=0$, thus

$$\prod_{i=2}^{m}\mu_i\int_0^t \mathrm{e}^{\alpha(t-s)}\mathsf{z}^T(s)\mathsf{z}(s)\mathrm{d}s < \prod_{i=2}^{m}\mu_i\int_0^t \mathrm{e}^{\alpha(t-s)}\gamma^2 v^T(s)v(s)\mathrm{d}s. \tag{C5}$$

Noting that

$$\int_0^t \mathsf{z}^T(s)\mathsf{z}(s)\mathrm{d}s < \prod_{i=2}^{m}\mu_i\int_0^t \mathrm{e}^{\alpha(t-s)}\mathsf{z}^T(s)\mathsf{z}(s)\mathrm{d}s;\ \ \prod_{i=2}^{m}\mu_i\int_0^t \mathrm{e}^{\alpha(t-s)}\gamma^2 v^T(s)v(s)\mathrm{d}s < \prod_{i=2}^{m}\mu_i\mathrm{e}^{\alpha t}\int_0^t \gamma^2 v^T(s)v(s)\mathrm{d}s. \tag{C6}$$

By setting $t=T_f$, it can be easily obtained

$$\int_0^{T_f} \mathsf{z}^T(s)\mathsf{z}(s)ds < \mathrm{e}^{\alpha T_f}\prod_{i=2}^{m}\mu_i\gamma^2\int_0^{T_f} v^T(s)v(s)\mathrm{d}s. \tag{C7}$$

Therefore, the NDSSs are H_∞ FTB with H_∞ performance index $\gamma^\star=\sqrt{\mathrm{e}^{\alpha T_f}\prod_{i=2}^{m}\mu_i}\gamma$. The proof is completed.

Appendix D Proof of Theorem 3

In conjunction with the above analysis of the sufficient conditions for H_∞ FTB, as discussed below, the matrix criteria for the systems (A2) to reach the LMIs form of H_∞ FTC are derived, and the piecewise state feedback controllers (PSFCs) are designed as well.

Theorem 3. Combining PSFCs, for given some positive constants d_1, β, T_f, m, α, l_{1i}, l_{2i}, γ, if there exist positive scalars $\mu_i>1$, ϵ_{fi}, ϵ_{gi}, ϵ_{ai}, ϵ_{di}, ϵ_{ei}, d_2, and positive definite matrices P_i, S_i, satisfying the following inequalities and the condition (C2), the closed-loop systems (A2) will be H_∞ FTC regarding (d_1, d_2, β, T_f, R, σ), with the same H_∞ performance index.

$$\begin{bmatrix}\Psi & \Sigma\\ * & \tilde{\Theta}\end{bmatrix}<0, \tag{D1}$$

$$X_j<\mu_i X_i, U_j<\mu_i U_i, j=i-1, \forall i,j\in\mathbb{M}, \tag{D2}$$

where

$$\Psi_{1,1}=\mathcal{A}_iX_i+X_i\mathcal{A}_i^T+\mathcal{G}Y_i+Y_i^T\mathcal{G}^T+\epsilon_{fi}I+\epsilon_{gi}I+\epsilon_{ai}H_{ai}H_{ai}^T+\epsilon_{di}H_{di}H_{di}^T-\alpha X_i, \Psi_{1,2}=\mathcal{A}_{di}U_i, \Psi_{1,3}=\mathcal{B},$$
$$\Psi_{1,4}=X_iE_i^T, \Psi_{2,2}=-(1-h)\mathrm{e}^{\alpha\iota}U_i, \Psi_{3,3}=-\gamma^2I, \Psi_{3,4}=\mathcal{W}^T, \Psi_{4,4}=-I+\epsilon_{ei}H_{ei}H_{ei}^T, \Sigma_{1,1}=\sqrt{l_{1i}}X_i, \Sigma_{1,3}=X_iM_{ai}^T,$$
$$\Sigma_{1,5}=X_iM_{ei}^T, \Sigma_{1,6}=X_i, \Sigma_{2,2}=\sqrt{l_{2i}}U_i, \Sigma_{2,4}=U_iM_{di}^T, \tilde{\Theta}=diag\{-\epsilon_{fi}I,-\epsilon_{gi}I,-\varepsilon_{ai}I,-\epsilon_{di}I,-\epsilon_{ei}I,-U_i\}.$$

By the design of PSFCs, the controllers' gain matrices are taken into account as $K_i=Y_iX_i^{-1}$.

Proof. Considering the systems, it follows from Theorem 2 that the matrix (C1) can be transformed into the following inequality with PSFCs applied

$$\tilde{\Pi}+\Delta_1^TL_{ai}^T(t)\Delta_2+\Delta_2^TL_{ai}(t)\Delta_1+\Delta_3^TL_{di}^T(t)\Delta_4+\Delta_4^TL_{di}(t)\Delta_3+\Delta_5^TL_{ei}^T(t)\Delta_6+\Delta_6^TL_{ei}(t)\Delta_5<0. \tag{D3}$$

According to Lemma 2, we have

$$\tilde{\Pi}+\epsilon_{ai}^{-1}\Delta_1^T\Delta_1+\epsilon_{ai}\Delta_2^T\Delta_2+\epsilon_{di}^{-1}\Delta_3^T\Delta_3+\epsilon_{di}\Delta_4^T\Delta_4+\epsilon_{ei}^{-1}\Delta_5^T\Delta_5+\epsilon_{ei}\Delta_6^T\Delta_6<0, \tag{D4}$$

where

$$\tilde{\Pi}_{1,1}=P_i\mathcal{A}_i+\mathcal{A}_i^TP_i+P_i\mathcal{G}K_i+K_i^T\mathcal{G}^TP_i+S_i+\epsilon_fP_i^2+\epsilon_gP_i^2-\alpha P_i, \tilde{\Pi}_{1,2}=P_i\mathcal{A}_{di}, \tilde{\Pi}_{1,3}=P_i\mathcal{B}, \tilde{\Pi}_{1,4}=E_i^T, \tilde{\Pi}_{1,5}=\sqrt{l_{1i}}I,$$
$$\tilde{\Pi}_{2,2}=-(1-h)\mathrm{e}^{\alpha\iota}S_i, \tilde{\Pi}_{2,6}=\sqrt{l_{2i}}I, \tilde{\Pi}_{3,3}=-\gamma^2I, \tilde{\Pi}_{3,4}=\mathcal{W}^T, \tilde{\Pi}_{4,4}=-I, \tilde{\Pi}_{5,5}=diag\{-\epsilon_{fi}I,-\epsilon_{gi}I\}, \Delta_1=(M_{ai},\underbrace{0,...,0}_{5}),$$
$$\Delta_2=(H_{ai}^TP_i,\underbrace{0,...,0}_{5}), \Delta_3=(0,M_{di},\underbrace{0,...,0}_{4}), \Delta_4=(H_{di}^TP_i,\underbrace{0,...,0}_{5}), \Delta_5=(M_{ei},\underbrace{0,...,0}_{5}), \Delta_6=(\underbrace{0,...,0}_{3},H_{ei}^T,\underbrace{0,...,0}_{2}).$$

Setting $X_i=P_i^{-1}$, $K_iX_i=Y_i$, $U_i=S_i^{-1}$, then employing Lemma 1 and multiplying the inequality (D4) before and after by $diag\{X_i,U_i,I_{7\times7}\}$ and its transpose, the condition (D1) implies that the above inequality (D4) holds. Moreover, the condition (D2) are similar as condition (C3). And the H_∞ performance index can be obtained similar to Theorem 2, so it's omitted here. Thus, the systems (A2) are H_∞ FTC with respect to (d_1, d_2, β, T_f, R, σ) via PSFCs.

Appendix E Switching strategies and optimization algorithm

Strategy 1. Considering the division of systems into subsystems according to time-averaged partitioning, it is assumed that the active time of the ith subsystem always equals that of the jth subsystem, which implies that $\delta_i = \delta_j$, $\forall i, j \in \mathbb{M}$, where $i \neq j$. Consequently, the upper and lower bounds for each subsystem are determined. In combination with the analysis of Theorem 3, the H_∞ FTC problem for NDSs is achieved.

Strategy 2. Under Strategy 1, it is natural to contemplate whether the average segmentation strategy would yield the minimum energy cost. Apparently, the reply is not certain. Therefore, this paper provides an optimization algorithm based on Grid search algorithm (GSA), on which the optimal segment points are sought globally, as see Algorithm E1 below. In contrast to Strategy 1, here $\delta_i \neq \delta_j$, $\forall i, j \in \mathbb{M}$, $i \neq j$. Afterward, upon acquisition of the optimization segment points, the delineation of the upper and lower bounds for each subsystem ensues, which in combination with Theorem 3 leads to the minimum energy cost and the solution of the H_∞ FTC problem.

An abbreviated algorithm is proposed in this paper that incorporates Strategy 2 and combines the Theorem 3, providing a practical implementation guide for understanding the results obtained.

Algorithm E1 GSA-based for minimum energy cost

Input: Given the scalars T_f and $\mathcal{J}_0$ solved by 1-stage feedback controller, choose $t_{1start} = 0.1$, $t_{2start} = 0.1 + \Delta t$ and Δt as the accuracy.
Output: The optimal energy cost $\mathcal{J}_1$ and the optimal switching points t_1, t_2.
1: **for** t_1 from t_{1start} to T_f by Δt. **do**
2: **for** t_2 from t_{2start} to T_f by Δt. **do**
3: **if** LMIs (D1)-(D2) are feasible, and solved $\mathcal{J}_1 < \mathcal{J}_0$. **then**
4: $\mathcal{J}_0 = \mathcal{J}_1$, and go back to step 1.
5: **else**
6: Go back to step 1.
7: **end if**
8: **end for**
9: **end for**
10: **return** The optimal energy cost $\mathcal{J}_1$.

Appendix F Numerical Simulations

It proffers three numerical instances to elucidate the validity of the presented switching strategies and Theorems. As the practical demonstrations, energy cost and performance of the controllers with different switching strategies can be evaluated to further support the claims and conclusions of this research.

Example 1. Considering the NDSs with Strategy 1 and the given parameters are shown as follows:

$$\mathcal{A}(t) = \begin{bmatrix} 0.5\cos(2t) - \frac{1}{1+t} & -1.7 \\ 1.22 & 0.44 + 0.5\cos(0.2t) \end{bmatrix}, \mathcal{G} = \begin{bmatrix} 0.5 \\ 0.15 \end{bmatrix}, \mathcal{A}_d(t) = \begin{bmatrix} 0.05\cos(t) + 0.05 & 0 \\ 0.1 & 0 \end{bmatrix}, \mathcal{B} = \begin{bmatrix} -0.0366 & 0.0271 \\ 0.0482 & -1.01 \end{bmatrix},$$

$$E(t) = \begin{bmatrix} 0 & 0.05\sin(0.4t) + 0.45 \\ 0.1 & 0 \end{bmatrix}, \mathcal{W} = \begin{bmatrix} -0.02 & 0.01 \\ 0 & -0.06 \end{bmatrix}, v(t) = \begin{bmatrix} 0.1\mathrm{e}^{-0.75t}\sin(t) \\ 0.2\mathrm{e}^{-0.2t}\cos(0.55t) \end{bmatrix}, \iota(t) = 0.7 + 0.05\sin(t).$$

the nonlinear functions are selected as $f(\mathsf{x}(t), t)$=0.1sin($\mathsf{x}(t)$), $g(\mathsf{x}(t-\iota(t)), t)$=0.05cos($\mathsf{x}(t-\iota(t))$)-0.05, and $l_{1i} = l_{2i} = 0.01$, $\forall i \in \mathbb{M}$. Considering $\iota = 0.75$, $h = 0.05$, $\beta = 0.057$, $\alpha = 0.01$, $\gamma = 1$, $d_1 = 0.37$, $t_0 = 0$ s, $T_f = 10$ s and $\mathsf{R} = I$, through Strategy 1, the solutions of Theorem 3 are calculated below.

Case 1. By regarding NDSs as regular time-varying systems, a 1-stage state feedback controller is employed.

$$X = \begin{bmatrix} 46.6686 & -0.6124 \\ -0.6124 & 0.6899 \end{bmatrix}, Y = \begin{bmatrix} -163.8285 & -75.6933 \end{bmatrix}, K = YX^{-1} = \begin{bmatrix} -5.0084 & -114.1559 \end{bmatrix}, U = \begin{bmatrix} 56.2124 & -1.1475 \\ -1.1475 & 29.7050 \end{bmatrix},$$

$\gamma^\star = \sqrt{\mathrm{e}^{\alpha T_f}}\gamma = 1.0513, \epsilon_a = 23.2206, \epsilon_d = 30.7309, \epsilon_e = 13.3375, \epsilon_f = 4.5879, \epsilon_g = 4.6210, \lambda_1 = 1.4667, \lambda_2 = 0.0337,$
$\lambda_3 = 0.0214, d_2 = 31.4512.$

Case 2. Average switching Strategy 1 is exploited to classify the NDSs into 2 subsystems relying on time-averaged segmentation for investigation and analysis. The switching time and parameter are selected as $t_1 = 5$ s and $\mu_2 = 1.85$, respectively.

$$X_1 = \begin{bmatrix} 24.4448 & -0.8521 \\ -0.8521 & 0.4957 \end{bmatrix}, Y_1 = \begin{bmatrix} -69.2114 & -41.6709 \end{bmatrix}, X_2 = \begin{bmatrix} 26.1886 & -1.0090 \\ -1.0090 & 0.9536 \end{bmatrix}, Y_2 = \begin{bmatrix} -87.4021 & -37.8048 \end{bmatrix},$$

$$K_1 = \begin{bmatrix} -6.1293 & -94.6071 \end{bmatrix} K_2 = \begin{bmatrix} -5.0717 & -45.0121 \end{bmatrix}, U_1 = \begin{bmatrix} 29.9120 & -0.7777 \\ -0.7777 & 15.6927 \end{bmatrix}, U_2 = \begin{bmatrix} 27.3997 & -0.7920 \\ -0.7920 & 16.9439 \end{bmatrix},$$

$\lambda_1 = 2.1487, \lambda_2 = 0.0639, \lambda_3 = 0.0381, \gamma^\star = 1.4299, d_2 = 46.6735, \epsilon_{a1} = 17.8725, \epsilon_{d1} = 16.7506, \epsilon_{e1} = 14.3422,$
$\epsilon_{f1} = 3.8555, \epsilon_{g1} = 3.8683, \epsilon_{a2} = 13.9247, \epsilon_{d2} = 16.6578, \epsilon_{e2} = 12.0906, \epsilon_{f2} = 2.8417, \epsilon_{g2} = 2.8225.$

Case 3. Similar to Case 2, Strategy 1 is applied to partition the NDSs into 3 subsystems depending on the time-averaged segmentation. The switching times and parameters are selected as $t_1 = 3.3$ s, $t_2 = 6.6$ s and $\mu_2 = 1.9$, $\mu_3 = 1.8$ respectively.

$$X_1 = \begin{bmatrix} 23.3495 & -0.8264 \\ -0.8264 & 0.5238 \end{bmatrix}, Y_1 = \begin{bmatrix} -65.9040 & -39.4400 \end{bmatrix}, X_2 = \begin{bmatrix} 24.3559 & -0.8936 \\ -0.8936 & 0.8378 \end{bmatrix}, Y_2 = \begin{bmatrix} -76.0201 & -37.3956 \end{bmatrix},$$

$$X_3 = \begin{bmatrix} 25.4560 & -1.1438 \\ -1.1438 & 1.1665 \end{bmatrix}, Y_3 = \begin{bmatrix} -84.0809 & -35.2437 \end{bmatrix}, K_1 = \begin{bmatrix} -5.8119 & -84.4586 \end{bmatrix}, K_2 = \begin{bmatrix} -4.9526 & -49.9171 \end{bmatrix},$$

$$K_3 = \begin{bmatrix} -4.8754 & -34.9944 \end{bmatrix}, U_1 = \begin{bmatrix} 28.9372 & -0.9431 \\ -0.9431 & 14.8300 \end{bmatrix}, U_2 = \begin{bmatrix} 26.9084 & -0.9485 \\ -0.9485 & 15.5682 \end{bmatrix}, U_3 = \begin{bmatrix} 26.4166 & -1.1650 \\ -1.1650 & 16.6163 \end{bmatrix},$$

$\lambda_1 = 2.0244, \lambda_2 = 0.0677, \lambda_3 = 0.0392, \gamma^\star = 1.9441, d_2 = 79.5303, \epsilon_{a1} = 18.4582, \epsilon_{d1} = 15.8417, \epsilon_{e1} = 13.6288,$
$\epsilon_{f1} = 3.9569, \epsilon_{g1} = 3.9733, \epsilon_{a2} = 15.9712, \epsilon_{d2} = 15.7723, \epsilon_{e2} = 14.5249, \epsilon_{f2} = 3.0721, \epsilon_{g2} = 3.0549, \epsilon_{a3} = 15.1212,$
$\epsilon_{d3} = 15.7513, \epsilon_{e3} = 12.5856, \epsilon_{f3} = 2.9168, \epsilon_{g3} = 2.8840.$

Energy cost for the three cases of **Example** 1 is shown in the Table F1 below.

Table F1 Energy cost by switching Strategy 1 and no switching

Controllers	1-stage	2-stage	3-stage
Energy cost	141.084	108.5024	95.3178
Improve efficiency (compared to 1-stage)		23.09%	32.44%

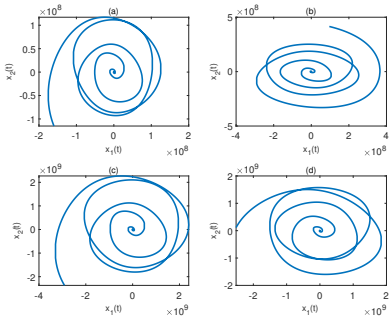

Figure F1 2D phase trajectories of NDSs without controller. (a) Trajectories with initial condition $\mathsf{x}_0 = [0, 0]^T$; (b) Trajectories with initial condition $\mathsf{x}_0 = [-0.1, 0.6]^T$; (c) Trajectories with initial condition $\mathsf{x}_0 = [-2, -5]^T$; (d) Trajectories with initial condition $\mathsf{x}_0 = [-4.1, -1.21]^T$.

Table F1 demonstrates the results of energy cost for two types of PSFCs exploiting Strategy 1 and 1-stage feedback controller. Presented outcomes reveal the effectiveness of Strategy 1 and satisfactory results achieved in energy conservation. Figure F1 visualizes the state diagrams with different initial conditions when NDSs remain uncontrolled. Figure F2(a) illustrates the state curves under the three types of controllers, while Figure F2(b) indicates that under three types of controllers, $\mathsf{x}^T(t)\mathsf{R}\mathsf{x}(t) < d_2$, which ensures that NDSs are FTB. Additionally, Figure F3(a) exhibits the curves of controllers. Figure F3(b) showcases the validity of H_∞ performance index under the zero initial value condition by 3-stage PSFC, assuring the system is H_∞ FTC.

Example 2. Set the same system conditions above in this example, which applies Strategy 2 and Algorithm E1 to derive the optimal switching points. Thereafter, the resolutions of Theorem 3 also can be computed below.

Case 1. Optimization Strategy 2 and Algorithm E1 are implemented to classify the NDSs into 2 subsystems. The optimized switching time parameter is assigned as $t_1 = 5.7$ s.

$$X_1 = \begin{bmatrix} 25.7530 & -0.8322 \\ -0.8322 & 0.5498 \end{bmatrix}, Y_1 = \begin{bmatrix} -73.7351 & -43.4801 \end{bmatrix}, X_2 = \begin{bmatrix} 26.7827 & -1.0385 \\ -1.0385 & 1.0311 \end{bmatrix}, Y_2 = \begin{bmatrix} -89.4430 & -38.3447 \end{bmatrix},$$

$$K_1 = \begin{bmatrix} -5.6973 & -87.7042 \end{bmatrix}, K_2 = \begin{bmatrix} -4.9758 & -42.1982 \end{bmatrix}, U_1 = \begin{bmatrix} 31.3612 & -0.6962 \\ -0.6962 & 15.8392 \end{bmatrix}, U_2 = \begin{bmatrix} 28.1568 & -0.8764 \\ -0.8764 & 17.1860 \end{bmatrix},$$

$\lambda_1 = 1.9144, \lambda_2 = 0.0633, \lambda_3 = 0.0373, \gamma^\star = 1.4299, d_2 = 42.9142, \epsilon_{a1} = 17.6023, \epsilon_{d1} = 16.9878, \epsilon_{e1} = 14.3061,$
$\epsilon_{f1} = 3.7738, \epsilon_{g1} = 3.7962, \epsilon_{a2} = 14.8524, \epsilon_{d2} = 16.8828, \epsilon_{e2} = 12.3535, \epsilon_{f2} = 2.9599, \epsilon_{g2} = 2.9409.$

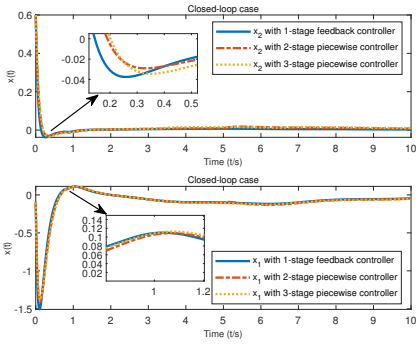

(a) State responses

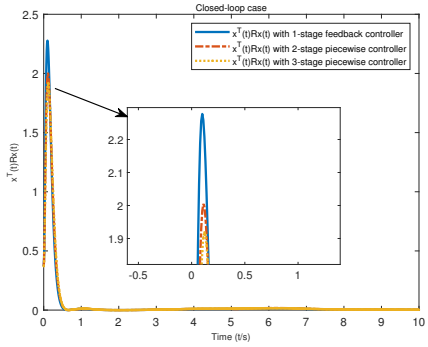

(b) $\mathsf{x}^T(t)\mathsf{R}\mathsf{x}(t)$

Figure F2 Simulation results with controllers. (a) State responses of $\mathsf{x}(t)$ employing Strategy 1 under three types of controllers with $\mathsf{x}_0 = [-0.1, 0.6]^T$; (b) Simulation results of $\mathsf{x}^T(t)\mathsf{R}\mathsf{x}(t)$ with Strategy 1.

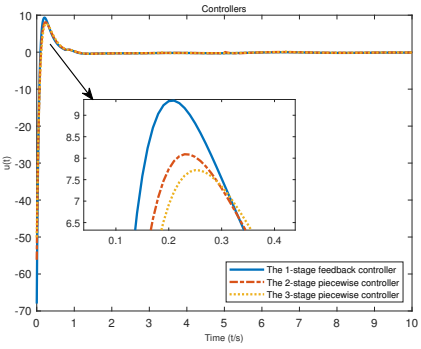

(a) Controllers

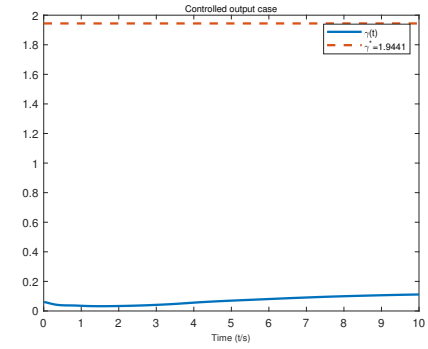

(b) $\gamma(t)$

Figure F3 Controllers and H_∞ performance index curves. (a) The trajectories of different controllers with Strategy 1; (b) Simulation results of $\gamma(t) = \sqrt{\frac{\int_0^t \mathsf{z}^T(s)\mathsf{z}(s)\mathrm{d}s}{\int_0^t v^T(s)v(s)\mathrm{d}s}}$, and $\gamma^\star = 1.9441$ with zero initial value by 3-stage average PSFC.

Case 2. As similar to Case 1, combining Strategy 2 with Algorithm E1 splits the NDSs into 3 subsystems. The optimized switching time parameters are quoted as $t_1 = 3.1$ s and $t_2 = 7.1$ s.

$$X_1 = \begin{bmatrix} 23.3438 & -0.7812 \\ -0.7812 & 0.5629 \end{bmatrix}, Y_1 = \begin{bmatrix} -65.7405 & -39.3616 \end{bmatrix}, X_2 = \begin{bmatrix} 24.7218 & -0.8521 \\ -0.8521 & 0.8533 \end{bmatrix}, Y_2 = \begin{bmatrix} -78.1367 & -37.6091 \end{bmatrix},$$

$$X_3 = \begin{bmatrix} 25.1448 & -1.1525 \\ -1.1525 & 1.2170 \end{bmatrix}, Y_3 = \begin{bmatrix} -82.9303 & -34.4624 \end{bmatrix}, K_1 = \begin{bmatrix} -5.4074 & -77.4313 \end{bmatrix}, K_2 = \begin{bmatrix} -4.8466 & -48.9124 \end{bmatrix},$$

$$K_3 = \begin{bmatrix} -4.8045 & -32.8662 \end{bmatrix}, U_1 = \begin{bmatrix} 28.8317 & -0.9542 \\ -0.9542 & 14.4811 \end{bmatrix}, U_2 = \begin{bmatrix} 26.9567 & -0.9929 \\ -0.9929 & 15.1911 \end{bmatrix}, U_3 = \begin{bmatrix} 26.1413 & -1.2283 \\ -1.2283 & 16.2360 \end{bmatrix},$$

$\lambda_1 = 1.8652, \lambda_2 = 0.0694, \lambda_3 = 0.0397, \gamma^\star = 1.9441, d_2 = 72.9667, \epsilon_{a1} = 18.2694, \epsilon_{d1} = 15.4600, \epsilon_{e1} = 13.2694,$
$\epsilon_{f1} = 3.8996, \epsilon_{g1} = 3.9166, \epsilon_{a2} = 14.9990, \epsilon_{d2} = 15.3914, \epsilon_{e2} = 13.6692, \epsilon_{f2} = 2.9037, \epsilon_{g2} = 2.8887, \epsilon_{a3} = 15.4217,$
$\epsilon_{d3} = 15.3366, \epsilon_{e3} = 12.6627, \epsilon_{f3} = 2.9415, \epsilon_{g3} = 2.9064.$

Energy cost and program running time for **Example** 2 are exhibited in Table F2 as follows.

Table F2 Energy cost by switching Strategy 2 and no switching

Controllers	1-stage	2-stage	3-stage
Energy cost	141.084	100.274	86.9794
Improve efficiency (compared to 1-stage)		28.93%	38.34%
Improve efficiency (compared to Strategy 1)		5.84%	5.9%
Running time	0.0019 h	0.2362 h	3.449 h

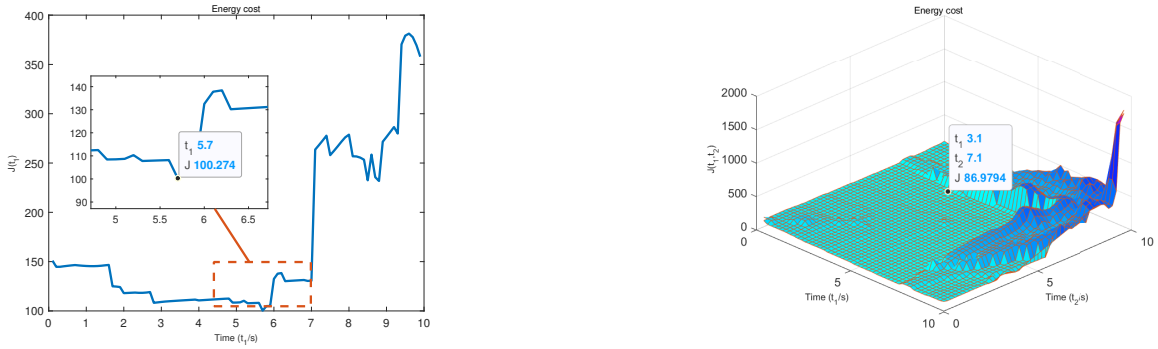

(a) $\mathcal{J}(t_1)$ (b) $\mathcal{J}(t_1, t_2)$

Figure F4 Energy cost simulation diagrams. (a) $\mathcal{J}(t_1)$ versus switching time t_1; (b) $\mathcal{J}(t_1, t_2)$ versus switching times t_1 and t_2.

The energy cost and program running time of the controllers at different stages with Strategy 2 are summarized in Table F2. Figures F4(a) and F4(b) simulate the result graphs for different switching times and energy cost in the effects of Strategy 2 and Algorithm E1, in which the global optimal points of energy cost are found. Figure F5 signifies the states with different initial conditions subjected to the optimized two types of controllers.

Remark 3. Noticeably, Tables F1 and F2 reveal that Strategy 2 is superior to Strategy 1, with more energy cost reductions for Strategy 2. It is clear from Table F2 that the more subsystems of NDSs are classified into, the lower energy cost will be. Besides, more subsystems make the implementation of the controller more complex and the program runtime more redundant. This implies that in practice the combination of control performance and complexity should be taken into account. For this application example, the optimized 2-stage PSFC is sufficiently suitable.

Example 3. From the analysis above, an example of the energy storing circuit is discussed below where we consider the application of the optimized 2-stage PSFC and 1-stage state feedback controller. A schematic diagram of the energy storing electrical circuit is presented as follows.

Figure F6 incorporates capacitance C, inductance L, variable resistors $R_1(t)$ and $R_2(t)$. Suppose that the state variables and the control input are taken as $\mathsf{x}(t) = [v_c, i_L]^T$ and $u(t) = V$ in which v_c and i_L indicate electric tension and electric current through the element, respectively. By considering $C = 1.4706, L = 5.556, R_1(t) = \frac{1+t}{0.5294(1+t)\cos(0.13t)+2.132}, R_2(t) =$

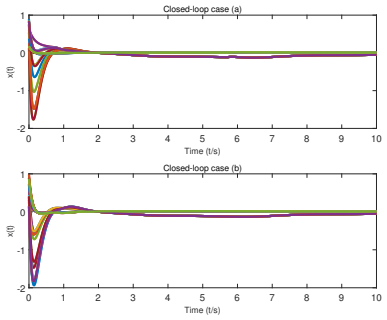

Figure F5 State responses of $\mathrm{x}(t)$ adopting Strategy 2 for 20 sets of different initial values. (a) State responses under the optimized 2-stage PSFC. (b) State responses under the optimized 3-stage PSFC.

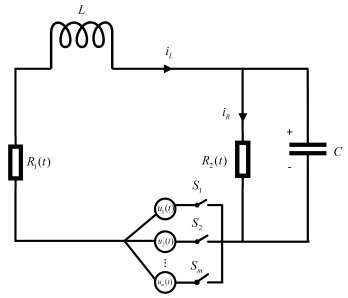

Figure F6 Schema of energy storing electrical circuit.

$2.445 + 1.389\cos(0.2t)$, for $t \in [0, 10]$, and the effects of time delays, nonlinear perturbations and the external disturbance, employing Kirchhoff laws, the following model is obtained.

$$\dot{\mathrm{x}}(t) = \mathcal{A}(t)\mathrm{x}(t) + \mathcal{A}_d(t)\mathrm{x}(t-\iota(t)) + f(\mathrm{x}(t),t) + g(\mathrm{x}(t-\iota(t)),t) + \mathcal{B}v(t) + \mathcal{G}u(t),$$

where

$$\mathcal{A}(t) = \begin{bmatrix} -0.36\cos(0.13t) - \frac{0.45}{1+t} & 0.68 \\ -0.18 & -0.44 - 0.25\cos(0.2t) \end{bmatrix}, \mathcal{G} = \begin{bmatrix} 0 \\ 0.18 \end{bmatrix},$$

with the other parameters are the same as in **Example** 1. Combining Strategy 2 and Algorithm E1, the optimized switching time parameter and switching parameter are chosen as $t_1 = 2.3$ s and $\mu_2 = 1.85$.

$$X = \begin{bmatrix} 1.9162 & -1.4829 \\ -1.4829 & 2.3034 \end{bmatrix}, Y = \begin{bmatrix} -2.2027 & -20.8395 \end{bmatrix}, X_1 = \begin{bmatrix} 4.0559 & -1.9786 \\ -1.9786 & 2.8506 \end{bmatrix}, Y_1 = \begin{bmatrix} -7.2177 & -34.1244 \end{bmatrix},$$

$$X_2 = \begin{bmatrix} 2.8829 & -1.7419 \\ -1.7419 & 4.1834 \end{bmatrix}, Y_2 = \begin{bmatrix} -2.1209 & -41.2336 \end{bmatrix}, K = \begin{bmatrix} -16.2430 & -19.5040 \end{bmatrix}, K_1 = \begin{bmatrix} -11.5202 & -19.9670 \end{bmatrix},$$

$$K_2 = \begin{bmatrix} -8.9403 & -13.5791 \end{bmatrix}, U = \begin{bmatrix} 7.7451 & -3.1191 \\ -3.1191 & 6.2653 \end{bmatrix}, U_1 = \begin{bmatrix} 14.2734 & -3.8846 \\ -3.8846 & 9.9029 \end{bmatrix}, U_2 = \begin{bmatrix} 15.1115 & -4.8646 \\ -4.8646 & 11.1892 \end{bmatrix},$$

$$\epsilon_a = 2.3929, \epsilon_d = 3.1466, \epsilon_e = 3.5424, \epsilon_f = 0.4199, \epsilon_g = 0.4154, \epsilon_{a1} = 6.3522, \epsilon_{d1} = 7.2969, \epsilon_{e1} = 7.1954,$$
$$\epsilon_{f1} = 1.5231, \epsilon_{g1} = 1.5033, \epsilon_{a2} = 3.9596, \epsilon_{d2} = 4.7194, \epsilon_{e2} = 4.8573, \epsilon_{f2} = 0.4327, \epsilon_{g2} = 0.4279.$$

Energy cost for **Example** 3 is indicated in Table F3 below.

Table F3 Energy cost by the optimized 2-stage PSFC and 1-stage controller

Controllers	1-stage	2-stage
Energy cost	2.1939	0.91933
Improve efficiency (compared to 1-stage)		58.096%

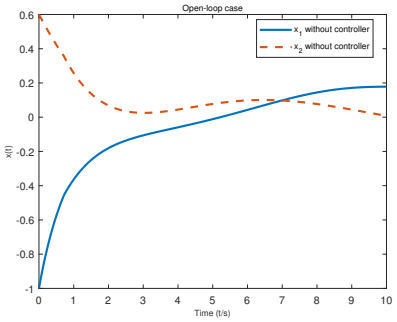

Figure F7 State trajectories of **Example** 3 without controller by $\mathrm{x}_0 = [-1, 0.6]^T$.

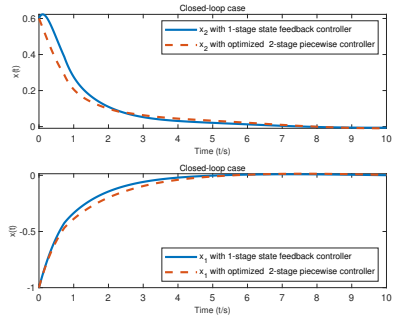

Figure F8 State trajectories of **Example** 3 with two types of controllers by $\mathrm{x}_0 = [-1, 0.6]^T$.

Table F3 demonstrates that the optimized 2-stage PSFC also contributes to reduced energy cost on the energy storing circuit example. Figure F7 illustrates the state diagram without controller, while Figure F8 shows state responses with the state feedback controller and the optimized 2-stage PSFC. Figure F9 depicts the trajectories of the optimized 2-stage controller and the state-feedback controller.

References

1 Amato F, Ariola M, Cosentino C. Finite-time stability of linear time-varying systems: analysis and controller design. IEEE Trans Automat Contr, 2010, 55: 1003-1008
2 Abdallah C T, Amato F, Ariola M, et al. Statistical learning methods in linear algebra and control problems: the example of finite-time control of uncertain linear systems. Linear Algebra Appl, 2002, 351: 11-26
3 Boyd S, El Ghaoui L, Feron E, et al. Linear matrix inequalities in system and control theory. Society for industrial and applied mathematics, 1994
4 Dong Y, Liu J, Mei S, et al. Stabilization for switched nonlinear time-delay systems. Nonlinear Anal Hybrid Syst, 2011, 5: 78-88
5 Amato F, Ariola M, Cosentino C. Finite-time stabilization via dynamic output feedback. Automatica, 2006, 42: 337-342
6 Zong G, Yang D, Hou L, et al. Robust finite-time H_∞ control for Markovian jump systems with partially known transition probabilities. J Frankl Inst, 2013, 350: 1562-1578
7 Xiang Z, Sun Y N, Mahmoud M S. Robust finite-time H_∞ control for a class of uncertain switched neutral systems. Commun Nonlinear Sci Numer Simul, 2012, 17: 1766-1778
8 Liu H, Zhao X. Finite-time H_∞ control of switched systems with mode-dependent average dwell time. J Frankl Inst, 2014, 351: 1301-1315

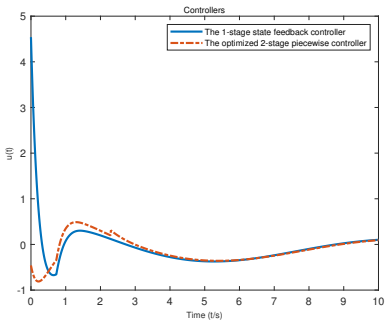

Figure F9 The trajectories of two types of controllers in **Example** 3.